

## Planar photonic crystals infiltrated with nanoparticle/polymer composites

Savaş Tay<sup>a)</sup> and Jayan Thomas<sup>b)</sup>

*College of Optical Sciences, The University of Arizona, Tucson, Arizona 85721, USA*

Babak Momeni, Murtaza Askari, and Ali Adibi

*School of Electrical and Computer Engineering, Georgia Institute of Technology, Atlanta, Georgia 30332 USA*

Peter J. Hotchkiss, Simon C. Jones, and Seth R. Marder

*School of Chemistry and Biochemistry and Center for Organic Photonics and Electronics, Georgia Institute of Technology, Atlanta, Georgia 30332, USA*

Robert A. Norwood and N. Peyghambarian

*College of Optical Sciences, The University of Arizona, Tucson, Arizona 85721, USA*

(Received 26 September 2007; accepted 5 November 2007; published online 29 November 2007)

Infiltration of planar two-dimensional silicon photonic crystals with nanocomposites using a simple yet effective melt processing technique is presented. The nanocomposites that were developed by evenly dispersing functionalized TiO<sub>2</sub> nanoparticles into a photoconducting polymer were completely filled into photonic crystals with hole sizes ranging from 90 to 500 nm. The infiltrated devices show tuning of the photonic band gap that is controllable by the adjustment of the nanoparticle loading level. These results may be useful in the development of tunable photonic crystal based devices and hybrid light emitting diodes and solar cells. © 2007 American Institute of Physics. [DOI: 10.1063/1.2817964]

Photonic crystals<sup>1</sup> (PCs) are engineered materials periodically arranged at the scale of the wavelength allowing the control of light by the creation of a photonic band gap, analogous to the electronic band gap in semiconducting crystals. The combination of PCs with the richness and flexibility of organic optical materials offer unique opportunities toward the development of high performance photonic devices. Significant research has been dedicated to the infiltration of PCs and other nanostructured materials with organic and hybrid optical materials as such systems pave the road for interesting applications such as tunable photonic circuits, electro-optic switches, organic lasers, high-*Q* cavity resonators, and hybrid light emitting diodes (LEDs) and solar cells.<sup>2–11</sup> Unusual physical properties such as control of spontaneous emission<sup>12</sup> can be demonstrated in PCs infiltrated with nanoparticle composites. Previously, several techniques for the infiltration of PCs with organic composites have been investigated.<sup>13–17</sup> However, specific problems, such as delamination and shrinkage of the infiltrants, have to be addressed if the full potential of many of these techniques are to be realized. For example, solution infiltration of PCs with polymers results in shrinkage and trapped air bubbles after the removal of solvents,<sup>13</sup> which increase optical losses and reduce device performance. Monomer infiltration<sup>13,16–18</sup> and subsequent polymerization can lead to a good degree of infiltration; however, the materials suitable for this approach are limited and oftentimes they experience 10%–15% of shrinkage after the thermally initiated polymerization.

To extend the materials and processes available for both linear and nonlinear PC devices, we have developed infiltrant nanocomposites and a simple technique based on melt processing of polymers for efficient infiltration into planar PCs and other nanoporous materials. The polymer chosen for nanocomposite development was an acrylate-

based material functionalized in the side chain with tetraphenyldiaminobiphenyl-type pendant groups (PATPD), as it has shown excellent results as the hole-conducting polymer in photorefractive composites.<sup>19,20</sup> Following a strategy recently reported,<sup>21</sup> we have tailored the nanoparticle surface modification chemistry to the composition of the polymer. A carbazole-functionalized phosphonic acid was synthesized and bound to commercially obtained TiO<sub>2</sub> nanoparticles (Aldrich) with an average diameter of 5 nm. This treatment afforded uniform dispersion of functionalized nanoparticles into the polymer melt, allowing the formation of homogeneous composites with nanoparticle loadings as high as 30 wt %. The functionalization of nanoparticles and nanocomposite development will be presented in detail in a further publication. The optical scattering from the nanocomposites was minimal even at the highest loading levels. The refractive indices of the PATPD/ *g*-ethylcarbazole (ECZ): TiO<sub>2</sub> nanocomposites were measured at 1550 nm using a prism coupler. For this, nanocomposites with different loadings of TiO<sub>2</sub> nanoparticles were prepared into thin films by sandwiching the melt at 185 °C between glass substrates followed by rapid cooling to suppress crystallization. The refractive index of the nanocomposite at this wavelength was found to increase with increasing nanoparticle loading in agreement with the Maxwell-Garnett effective medium theory, reaching 1.74 at a loading of 30 wt %. This constitutes an increase of 0.08 compared to the refractive index of the nanoparticle-free PATPD/ECZ polymer.

A melt infiltration technique was adopted to fill the holes of photonic crystals. First, high viscosity polymers and nanocomposite materials were converted into low *T<sub>g</sub>*, low viscosity composites by the use of the plasticizer ECZ. These nanocomposites were then heated to temperatures above their melting point for infiltration. Silicon PC substrates with hole sizes ranging from 90 to 500 nm were fabricated by e-beam lithography and used for infiltration. The substrates were cleaned using a piranha solution followed by rinsing in an

<sup>a)</sup>Electronic mail: savas.tay@optics.arizona.edu.

<sup>b)</sup>Electronic mail: jthomas@optics.arizona.edu.

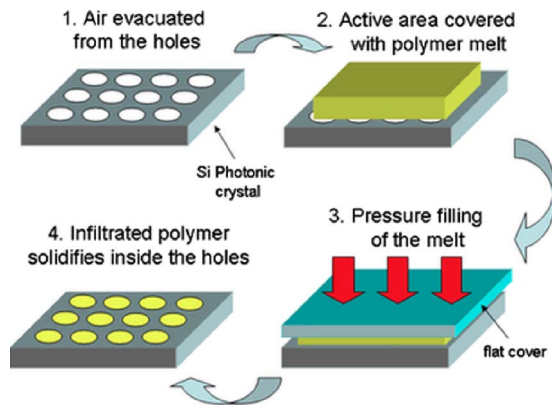


FIG. 1. (Color online) Polymer infiltration of PCs using melt processing: (1) air is evacuated from the holes of the photonic crystal, (2) the holes are covered with the polymer and heated above its melting temperature, (3) the polymer melt is forced into the holes using mechanical pressure, and (4) the polymer is rapidly cooled to avoid crystallization.

ammonia/hydrogen peroxide solution. This treatment results in a low contact angle between the polymer melts and the silicon surface indicative of good wetting. An evacuated chamber was utilized to remove most of the air from the PC holes, and the remaining steps of infiltration were performed inside this chamber. The nanocomposite, PATPD/ECZ:TiO<sub>2</sub> with 30 wt % TiO<sub>2</sub> particle loading, was then melted into the holes by heating the substrate on a hot plate and applying mechanical pressure (Fig. 1). The filled PC device was rapidly cooled down to room temperature, allowing for the solidification of the nanocomposite. The infiltrated devices were cleaved and investigated using scanning electron microscopy (SEM). Complete filling for all hole sizes from 90 up to 500 nm was achieved using this simple technique as evidenced by SEM side views of the infiltrated holes (Fig. 2). The nanocomposites fill the holes conformally without shrinkage and remain intact for at least months without delamination from the sidewalls. The nanoparticles are evenly dispersed into the holes of the PC without any noticeable aggregation. The nanocomposite film covering the top of the devices has a thickness around 2 μm and is extremely flat. Such a melt-based process as described here has significant advantages over solvent-based approaches as it is simple, flexible, results in defect-free infiltration, and has low inherent material loss.

Infiltration of PCs with high index nanocomposites can be used for tuning the photonic band-gap. To characterize the optical properties of the material and the quality of the infiltration process, we have examined the stop band of planar PCs infiltrated with polymers or polymer/nanoparticle composites for comparison. The PCs consist of a square lattice array of air holes etched through the top silicon layer of silicon-on-insulator wafers. The lattice constant of the PC in the fabricated structures is 370 nm, the etched holes have a diameter of 220 nm, and the thickness of the top silicon layer in the final structure is 220 nm. To measure the transmission response of the PC, a ridge waveguide with a width of 4.8 μm was used to bring the light to the PC region. This input waveguide was gradually tapered from an initial single-mode width to its final width so that the input light to the PC structure consists mainly of the lowest-order mode of the input ridge waveguide. The light passes through 20 μm of PC, and the output was coupled to another ridge waveguide that carries the light to the end face of the sample. The end face of the sample was imaged using an objective lens to a detector. The detector and tunable laser were both connected to a lock-in amplifier for improving the signal-to-noise ratio of the measurement. The insertion loss of the device is less than 20 dB/mm without polymer infiltration, similar to the PC devices reported previously. Figure 3(a) shows the measurement results for the two cases in which the holes of the planar PC were filled with the reference polymer (PATPD/ECZ) or the TiO<sub>2</sub> nanoparticle loaded polymer (PATPD/ECZ:TiO<sub>2</sub>). In these measurements, TE-like polarization was used for the input light. In both cases, the contrast between the high transmission in the passband of the PC structure and the low transmission in the stop band of the PC is around 20 dB. This high contrast indicates that the filling of the PC holes is complete and uniform, and as a result, the PC stopband is pronounced and the scattering from partially filled holes is negligible. The infiltrated samples do not show any increased optical loss indicating the high quality of the nanocomposite and the infiltration process. Furthermore, by comparing the two plots in Fig. 3(a), it can be observed that the passband (and thereby, the edge of the PC stop band) is shifted toward longer wavelengths when the polymer contains 30 wt % TiO<sub>2</sub> nanoparticles. This indicates that the PATPD/ECZ:TiO<sub>2</sub> nanocomposite has effectively a higher

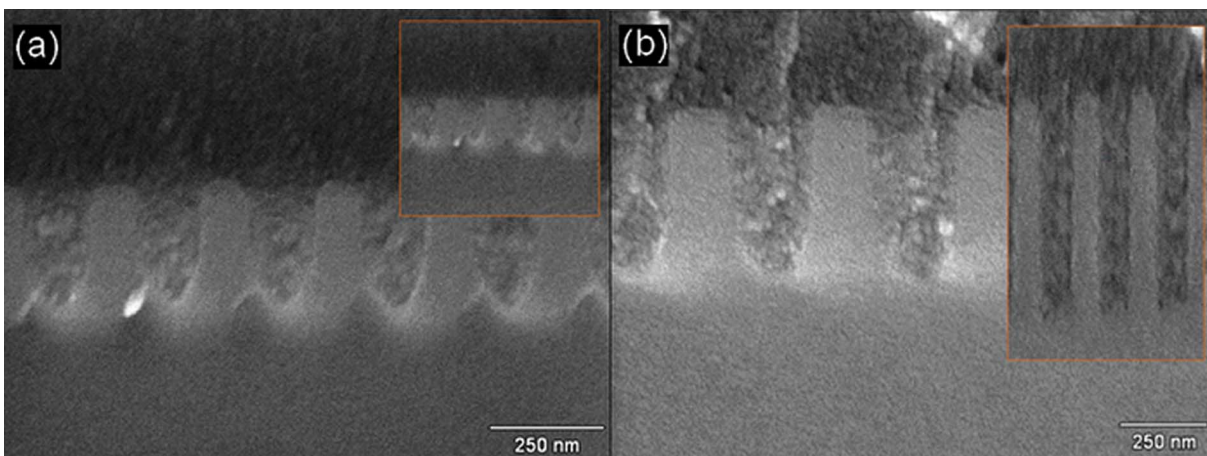


FIG. 2. (Color online) (a) Cross sectional SEM images of polymer infiltrated holes of a PC. The holes are completely filled with the polymer PATPD, and the PC is cleaved along a crystal axis; this creates some artifacts on the polymer surface. Inset shows the same holes four weeks after the infiltration indicating no delamination of the polymer. (b) Different sized holes filled with the PATPD/ECZ:TiO<sub>2</sub> (30 wt % nanoparticle loading) nanocomposite. Inset shows 90 nm wide holes completely filled with the nanocomposite. The nanoparticles are homogeneously distributed without visible aggregation.

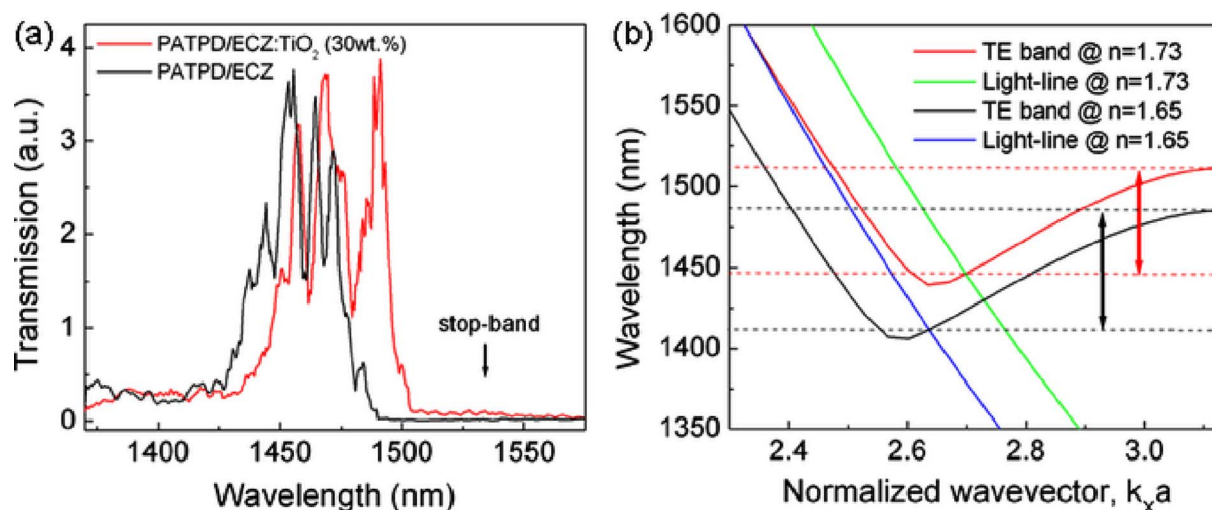


FIG. 3. (Color online) (a) Transmission measurements for the two PCs infiltrated with PATPD/ECZ polymer (black curve) or the PATPD/ECZ:TiO<sub>2</sub> nanocomposite (red curve). The loading level of the TiO<sub>2</sub> nanoparticles was 30 wt %. The edge of the transmission band above 1500 nm is due to the photonic stop band of the PC, and the one below 1425 nm corresponds to the light-line crossing. The shift in the transmission band arises from the difference between the refractive indices of the materials used for filling. (b) Calculated band structures of the PC shown in (a) with different refractive indices inside the holes. The arrows show the calculated passband in each case. The calculated values agree well with the measured transmission bands shown in (a).

refractive index compared to PATPD alone. To verify this effect, the band structure of the PC in the  $\Gamma X$  direction (i.e., along the direction excited by the incident beam in our PC structure) was calculated using a standard three-dimensional supercell plane-wave expansion method as shown in Fig. 3(b). In the band structure plotted in Fig. 3(b), only the TE-like mode that is excited in the measurement setup is retained. A numerical extrapolation was employed to improve the convergence of this plane-wave expansion method. The refractive indices of the top polymer layer for the two cases shown in Fig. 3 are assumed to be 1.65 (black line) and 1.73 (red line) as obtained from the direct measurement by prism coupling. The calculations predict the band edge of the gap to shift from 1487 to 1510 nm, as plotted in Fig. 3(b), and these values are in agreement with the experimentally observed shift from 1485 to 1505 nm shown in Fig. 3(a). The agreement between the results obtained from the experiments with those in the simulations confirms the validity of the assumed change in the nanocomposite refractive index. Moreover, we can see that the theoretical expectations and experimental results are in good agreement in providing the onset of the transmitted (leaky) modes (where the PC modes are above the light line), which is further the proof for both the validity of representing the PATPD/ECZ:TiO<sub>2</sub> nanocomposite with an effective refractive index and the absence of significant light scattering due to partially filled holes or nanoparticle aggregates.

In conclusion, we have used a simple yet effective method based on melt processing of polymers for the infiltration of nanostructured semiconductor PC devices with organic nanocomposites. Highly homogenous polymer/nanoparticle composites suitable for use in hybrid photonic applications were used to completely fill the air holes of two-dimensional silicon PCs. The infiltration of the PCs with the nanocomposites results in the controllable shift of the photonic band-gap which may have important applications in tunable PC-based technologies, hybrid LEDs, and photovoltaics.

This work was supported by the Office of Naval Research APEX program, the National Science Foundation's MDITR STC, and the US Air Force Office of Scientific

Research. We thank Kevin Sandhage for use of his TGA and Johannes Leisen for help in NMR measurements.

- <sup>1</sup>J.-M. Lourtioz, H. Benisty, V. Berger, J.-M. Gérard, D. Maystre, and A. Tchebnokov, *Photonic Crystals: Towards Nanoscale Photonic Devices* (Springer, New York, 2003).
- <sup>2</sup>K. Busch and S. John, *Phys. Rev. Lett.* **83**, 967 (1999).
- <sup>3</sup>S. F. Mingaleev, M. Schillinger, M. Hermann, and K. Busch, *Opt. Lett.* **29**, 2858 (2004).
- <sup>4</sup>M. Schmidt, M. Eich, U. Huebner, and R. Boucher, *Appl. Phys. Lett.* **87**, 121110 (2005).
- <sup>5</sup>K. Inoue, M. Sasada, J. Kawamata, K. Sakoda, and J. W. Haus, *Jpn. J. Appl. Phys., Part 2* **38**, L157 (1999).
- <sup>6</sup>J. R. Lawrence, Y. Ying, P. Jiang, and S. H. Foulger, *Adv. Mater. (Weinheim, Ger.)* **18**, 300 (2006).
- <sup>7</sup>S. Tomljenovic-Hanic, C. M. de Sterke, and M. J. Steel, *Opt. Express* **14**, 12451 (2006).
- <sup>8</sup>S.-K. Lee, G.-R. Yee, J. H. Moon, S.-M. Yang, and D. J. Pine, *Adv. Mater. (Weinheim, Ger.)* **18**, 2111 (2006).
- <sup>9</sup>S. Furumi, H. Fudoizi, H. T. Miyazaki, and Y. Sakka, *Adv. Mater. (Weinheim, Ger.)* **19**, 2067 (2007).
- <sup>10</sup>Y.-C. Kim and Y. R. Do, *Opt. Express* **13**, 1598 (2005).
- <sup>11</sup>B. Kannan, K. Castelino, and A. Majumdar, *Nano Lett.* **3**, 1729 (2003).
- <sup>12</sup>P. Lodahl, A. Floris van Driel, I. S. Nikolaev, A. Irman, K. Overgaag, D. Vanmaekelbergh, and W. L. Vos, *Nature (London)* **430**, 654 (2005).
- <sup>13</sup>R. van der Heijden, C. F. Carlstöm, J. A. P. Snijders, R. W. van der Heijden, F. Karouta, R. Nötzel, H. W. M. Salemink, B. K. C. Kjellander, C. W. M. Bastiaansen, D. J. Broer, and E. van der Drift, *Appl. Phys. Lett.* **88**, 161112 (2006).
- <sup>14</sup>M. Deutsch, Y. A. Vlasov, and D. Norris, *Adv. Mater. (Weinheim, Ger.)* **12**, 1176 (2000).
- <sup>15</sup>C. López, *Adv. Mater. (Weinheim, Ger.)* **15**, 1679 (2003).
- <sup>16</sup>A. Yu, F. Meiser, T. Cassagneau, and F. Caruso, *Nano Lett.* **4**, 172 (2004).
- <sup>17</sup>J.-H. Park, W. S. Choi, H. Y. Koo, and D.-Y. Kim, *Adv. Mater. (Weinheim, Ger.)* **17**, 879 (2005).
- <sup>18</sup>Y. J. Jung, S. Kar, S. Talapatra, C. Soldano, G. Viswanathan, X. Li, Z. Yao, F. S. Ou, A. Avadhanula, R. Vajtai, S. Curran, O. Nalamasu, and P. M. Ajayan, *Nano Lett.* **6**, 413 (2006).
- <sup>19</sup>J. Thomas, C. Fuentes-Hernandez, M. Yamamoto, K. Cammack, K. Matsumoto, G. A. Walker, S. Barlow, B. Kippelen, G. Meredith, S. R. Marder, and N. Peyghambarian, *Adv. Mater. (Weinheim, Ger.)* **16**, 2032 (2004).
- <sup>20</sup>S. Tay, J. Thomas, M. Eralp, G. Li, R. A. Norwood, A. Schulzgen, M. Yamamoto, S. Barlow, G. A. Walker, S. R. Marder, and N. Peyghambarian, *Appl. Phys. Lett.* **87**, 171105 (2005).
- <sup>21</sup>P. Kim, S. C. Jones, P. J. Hotchkiss, J. N. Haddock, B. Kippelen, S. R. Marder, and J. W. Perry, *Adv. Mater. (Weinheim, Ger.)* **19**, 1001 (2007).